Ionization energies and electron affinities from a random-phase-approximation many-body Green's-function method including exchange interactions

Andreas Heßelmann
Lehrstuhl für Theoretische Chemie, Universität Erlangen-Nürnberg, Egerlandstrasse 3, D-91058 Erlangen, Germany
(Received 27 March 2017; published 28 June 2017)

A many-body Green's-function method employing an infinite order summation of ring and exchange-ring contributions to the self-energy is presented. The individual correlation and relaxation contributions to the quasiparticle energies are calculated using an iterative scheme which utilizes density fitting of the particle-hole, particle-particle and hole-hole densities. It is shown that the ionization energies and electron affinities of this approach agree better with highly accurate coupled-cluster singles and doubles with perturbative triples energy difference results than those obtained with second-order Green's-function approaches. An analysis of the correlation and relaxation terms of the self-energy for the direct- and exchange–random-phase-approximation (RPA) Green's-function methods shows that the inclusion of exchange interactions leads to a reduction of the two contributions in magnitude. These differences, however, strongly cancel each other when summing the individual terms to the quasiparticle energies. Due to this, the direct- and exchange-RPA methods perform similarly for the description of ionization energies (IPs) and electron affinities (EAs). The coupled-cluster reference IPs and EAs, if corrected to the adiabatic energy differences between the neutral and charged molecules, were shown to be in very good agreement with experimental measurements.

DOI: 10.1103/PhysRevA.95.062513

I. INTRODUCTION

Molecular ionization energies (IPs) and electron affinities (EAs) can be determined with a high accuracy using experimental measurements, e.g., photoelectron spectroscopy [1–3] or electron impact experiments [4,5]. Because of this, these properties serve well as reference data for testing the accuracy of quantum chemistry electron correlation methods. In the case of the latter, principally two main approaches exist to determine IPs and EAs. In the first one the IPs or EAs are calculated from the energy differences between the charged and neutral molecules according to

$$\Delta E^{\mathrm{IP}} = E^{\mathrm{cation}} - E^{\mathrm{neutral}}, \tag{1}$$

$$\Delta E^{\mathrm{EA}} = E^{\mathrm{neutral}} - E^{\mathrm{anion}}. \tag{2}$$

The advantage of this approach is that it can principally be used in conjunction with any quantum chemical method which provides energies for the closed- and open-shell systems and, by construction, takes relaxation and correlation effects for the N- and $(N+1)/(N-1)$-electronic systems fully into account through all orders of a many-body expansion of the energy difference. A disadvantage of the energy difference method of Eqs. (1) and (2) is, however, that separate energy calculations are required to compute single, double, triple, etc., ionizations or electron attachment energies, so that this approach becomes very expensive if the full quasiparticle spectrum is desired.

This can be resolved by a direct determination of the IPs and EAs using many-body Green's-function methods [6–18]. In these methods, in contrast to standard wave-function approaches, the electronic Schrödinger equation is solved by a transformation into an integral equation containing the resolvent to the Hamiltonian. A knowledge of this quantity, denoted as the Green's function of the many-body system, could then be used to directly determine a range of molecular properties, including ground-state energies [19–21], transition matrix elements [22], absorption coefficients [23], dynamic polarizabilities [14,24], phonon spectra [25], as well as elastic and inelastic cross sections [26]. Furthermore, ionization energies and electron affinities of the N-particle system, that are the quantities of interest in this work, can be obtained by determining the poles of the Green's function [27].

Since the Green's function (GF) in general is an unknown quantity, it has to be approximated in practice. This usually is done by solving the Dyson integral equation which relates the Green's function of a noninteracting many-body system to a fully interacting system by taking into account screened interactions through an energy-dependent potential termed as self-energy. As described in Ref. [28], the name self-energy originates from the mutual interactions of a single particle with the many-body system and describes the difference between the energy of the bare particle and the energy of the particle plus a surrounding cloud of agitated particles screening the interactions in the system. The sum of the particle with its cloud is also denoted as a quasiparticle.

The simplest quasiparticle approach is obtained by taking into account first-order electron-electron interactions, leading to the Hartree-Fock (HF) approximation. In this approximation (and any other effective one-particle theories) the Green's function can explicitly be expressed in terms of the HF orbitals (ϕ_r) and orbital energies (ε_r):

$$G_0(\mathbf{r}_1,\mathbf{r}_2,\omega) = \sum_r \frac{\phi_r(\mathbf{r}_1)\phi_r^{\dagger}(\mathbf{r}_2)}{\omega - \varepsilon_r}. \tag{3}$$

As can be seen in Eq. (3), the HF Green's function possesses poles at the HF orbital energies. These are related to the IPs and EAs of the N-particle system due

to Koopman's theorem. Accordingly, as noted above, the exact one-particle many-body Green's function has poles at the exact (vertical) IPs and EAs of the many-body system.

Like in standard wave function theories, the unknown self-energy potential can be approximated using perturbation theory approaches, starting from the HF approximation as the zeroth order self-energy contribution [27,29]. With this the (energy independent) Coulomb and first-order exchange interactions are separated from the self-energy potential and the latter then solely describes the remaining correlation and relaxation contributions to the quasiparticle energies.

Perturbation theory approaches to the many-body Green's function method have been developed by a number of groups using a second- [12,30–33], third- [8,9,13,16,18,34], or even fourth-order [35] expansion of the self-energy with respect to the electron-electron interaction. It has been found that third-order methods usually provide IPs and EAs which are in reasonable agreement with experimental reference results [13,17,18,36]. Even higher accuracies are obtained by infinite order approaches like the coupled-cluster Green's-function method by Nooijen and Snijders [37,38]. Note also that many-body Green's-function methods can be related to equation-of-motion coupled-cluster methods [39] and Fock-space coupled-cluster methods [39,40]. In the case of the latter, the quasiparticle energies can be calculated from an effective one-particle electron correlation method employing an energy-independent correlation potential which transforms the orbitals to Brueckner orbitals [39]. The close relation between many-body perturbation theory methods based on an effective one-particle Brueckner model space and Green's-function methods has also been discussed by Lindgren [41] and Ortiz [42].

Another approach to calculate the self-energy potential is the Hedin GW method which aims at determining an approximate solution to Hedin's equations [43–45]. These form a set of four coupled equations which relate the self-energy, the screened interaction, the polarization function, and the vertex function [43,44,46]. While the derivation of an exact solution to these equations, in combination with the Dyson equation, would yield the exact one-particle propagator, in practice this would be a quite demanding task from a computational point of view. Because of this, in the GW method the vertex function is approximated to be diagonal in space and time coordinates. With this it is described by the product of the Green's function and the dynamically screened Coulomb interaction [43,46]. It should be noted, however, that still the GW method constitutes a many-body self-consistent problem which has to be solved. Typical further approximations to the GW method are the non-self-consistent G_0W_0 method in which the Green's function is modeled by the noninteracting G_0 and the screened interaction is kept at the RPA level, and the GW_0 self-consistent approach on G [20,47].

In a non-self-consistent GW method also the zeroth-order approximation to the Green's function can have a significant influence on the accuracy of the method. Above it has been argued that the Hartree-Fock method is a good starting point for deriving corrections to the self-energy due to the fact that the HF orbital energies are already related to ionization energies and electron affinities of the N-particle system due to Koopman's theorem. In the case of the Kohn-Sham pseudoparticle system a related theorem can also be derived for the occupied orbitals [48] while, however, the eigenvalues of unoccupied Kohn-Sham orbitals are not associated with electron affinities but to the ionization energies of the anionic systems [49]. In spite of this, GW calculations are conventionally carried out in conjunction with Kohn-Sham references, in particular for calculating the quasiparticle spectrum of bulk semiconductors and insulators [44,50,51]. Kohn-Sham GW calculations for molecular systems have been implemented and tested by Shigeta *et al.* [52] and more recently by van Setten and co-workers [53–56]. Fully self-consistent GW methods for molecules have been developed by Rostgaard *et al.* [57] and Koval *et al.* [58]. In the work by Rostgaard *et al.* a comparison between HF-based and KS-based GW methods is made [57]. It was found that at the G_0W_0 level HF GW methods are more accurate than KS GW methods. At full self-consistency, however, the results for quasiparticle energies are almost independent on the starting reference [57,58].

In this work a diagrammatic method is presented which enables the computation of the self-energy potential through infinite order within the random-phase approximation (RPA) including all particle-hole exchange interactions. This method, termed as the RPAX2 method in Ref. [59], has recently been implemented for obtaining the ground-state correlation energies of molecules using a Kohn-Sham reference state. Thermokinetic molecular properties, including ionization energies and electron affinities, were shown to be very accurate with the Kohn-Sham based RPAX2 method [60]. Here, however, a Hartree-Fock reference will be used as the zeroth-order approximation to the many-body Green's function. This has the advantage that the correlation contributions to the IPs and EAs obtained by the RPA or RPAX2 approaches can directly be interpreted as corrections to Koopman's theorem. While a corresponding theorem also exists for the occupied energy levels of the "exact" KS method, as noted above, in general the exact KS potential is unknown and has to be approximated. Exchange-correlation potentials from standard generalized-gradient approximation functionals, however, yield orbital energies which strongly underestimate the negative ionization energies of the N-particle system due to an incorrect asymptotic behavior of the exchange-correlation potential [52,61]. This is only partially resolved by using hybrid functionals and therefore either an asymptotic correction method [61–65], or a more sophisticated orbital-dependent KS functional using the optimized-effective potential method [66–71] would have to be used to obtain a reasonable description of the zeroth-order Green's function.

The methods considered in this work will be tested for a recently developed set of 27 benchmark systems for studying the performance of GW methods [53]. Geometries as well as reference IPs and EAs for this GW27 database have been revised in this work using the MP2 method for the structure optimizations and complete basis set extrapolated CCSD(T) energies for obtaining accurate IPs and EAs. It is shown that these results, if corrected to the adiabatic

energy differences between the charged and neutral systems, are in a very good agreement with experimental measurements. They may therefore serve well as reference data for testing other quantum chemistry (Green's-function) methods.

Correlation and relaxation effects to the self-energy potential are treated separately in the approach of this work. This will enable us to analyze the influence of these two contributions on the quasiparticle energies and may generally be useful for characterizing the electronic structure of the molecule.

This work is organized as follows: Section II describes the methods of this work using a diagrammatic approach that is outlined in Sec. II B 1. Section III summarizes the computational details for the calculations done. In Sec. IV the results are presented. Here it is first shown that the CCSD(T) reference values compare well with experimental IPs and EAs in Sec. IV A. In Sec. IV B differences between the quasiparticle energy levels of some Green's-function methods are investigated for a selection of molecules of the GW27 database, discussing also the influence of correlation, relaxation, and static self-energy contributions to the magnitudes of the energy levels. In the final subsection of the results section, Sec. IV C, the IPs and EAs from the approaches of this work as well as other standard wave-function methods are compared against the coupled-cluster reference results. Section V summarizes the results.

II. METHOD

A. Poles of the many-body Green's function

The Green's function $\mathbf{G}(\omega)$ of an interacting many-body system can be calculated by solving the Dyson integral equation, which, in a matrix representation, reads [27]

$$\mathbf{G}(\omega) = \mathbf{G}_0(\omega) + \mathbf{G}_0(\omega)\mathbf{\Sigma}(\omega)\mathbf{G}(\omega), \tag{4}$$

where ω is the quasiparticle energy, $\mathbf{G}_0(\omega)$ is the Hartree-Fock (HF) Green's function, and $\mathbf{\Sigma}(\omega)$ is the exact self-energy in the basis of the HF orbitals. It can be shown that $\mathbf{G}_0(\omega)$ has poles at the HF orbital energies which are related to the ionization potentials (IPs) and electron affinities (EAs) of the N-particle system through Koopman's theorem [27]. Correspondingly, the many-body Green's function $\mathbf{G}(\omega)$ possesses poles at the exact energy differences between the N particle and $(N-1)$ particle respectively $(N+1)$-particle system, i.e., the exact IPs and EAs.

In this work only the poles of $\mathbf{G}(\omega)$ shall be considered. For this, note that Eq. (4) can be recast into [27]

$$\mathbf{G}(\omega) = \frac{\mathbf{1}}{\omega\mathbf{1} - \boldsymbol{\varepsilon} - \mathbf{\Sigma}(\omega)}, \tag{5}$$

where $\boldsymbol{\varepsilon}$ is a diagonal matrix containing the occupied and virtual HF orbital energies. This form of the Green's function now clearly shows that $\mathbf{G}(\omega)$ reduces to $\mathbf{G}_0(\omega)$ if $\mathbf{\Sigma}(\omega) = \mathbf{0}$. If many-body interactions beyond first order are taken into account, it follows from Eq. (5) that generalized single-particle equations of the form

$$[\hat{f} + \hat{\Sigma}(\omega)]\phi_i^{\mathrm{Dyson}}(\mathbf{r},\omega) = \omega\phi_i^{\mathrm{Dyson}}(\mathbf{r},\omega) \tag{6}$$

have to be solved. In Eq. (6) $\hat{f}$ denotes the Fock operator and ϕ_i^{Dyson} corresponds to the Dyson orbital of the ith state. While having a form almost identical to the HF single-particle equations, note that the self-energy operator $\hat{\Sigma}(\omega)$ is energy dependent and thus the above equation represents a non-Hermitian eigenvalue problem. Accordingly, the Dyson orbitals form in general a nonorthonormal set of single-particle states.

In order to arrive at a computational tractable form, two approximations are now introduced. First, the off-diagonal elements of the matrix $\boldsymbol{\varepsilon} + \mathbf{\Sigma}(\omega)$ shall be neglected, so that the poles of $\mathbf{G}(\omega)$ can directly be obtained from the equation

$$\omega = \varepsilon_i + \Sigma_{ii}(\omega). \tag{7}$$

The impact of this approximation on quasiparticle energy levels has, e.g., been studied in Refs. [72,73]. Kaplan *et al.* have shown in Ref. [72] that, as compared to a self-consistent update of the poles, the inclusion of the off-diagonal terms in G_0W_0 calculations has only a small effect on the ionization energies for a range of small molecules. In Ref. [73] Beste and Bartlett have used the diagonal approximation within a second-order Brueckner correlation method. The ionization energies and electron affinities (estimated by the occupied and unoccupied orbital energies) obtained by this approach were shown to be almost identical to those obtained from a diagonalization of the occupied-occupied and virtual-virtual blocks of the Brueckner Hamiltonian. Due to this, it can be assumed that Eq. (7) is a reasonable approximation to determine the quasiparticle poles within a given orbital space.

As can be seen in Eq. (7), the poles of the Green's function can now easily be obtained by iterating the above equation using $\omega_0 = \varepsilon_i$ as an initial guess [27]. Via this, while Eq. (7) can have many solutions, the pole of the Green's function that is retained by this starting guess should be the one which possesses the largest strength (provided that the initial Hartree-Fock orbital energies are close to the exact quasiparticle energies). It was found in this work that within the diagonal approximation the converged solutions to Eq. (7) differed only slightly from the first-order solution,

$$\omega = \varepsilon_i + \Sigma_{ii}(\varepsilon_i), \tag{8}$$

and thus Eq. (8) will be used in this work to approximate the poles of $\mathbf{G}(\omega)$.

B. Self-energy matrix within the random-phase approximation

1. Diagrammatic approach

In this work, the method to compute the diagonal self-energy matrix elements is derived by using a diagrammatic approach. The corresponding algebraic expressions to the diagrams displayed in the equations below are given in the Supplemental Material [74]. The main building blocks of the Goldstone-type diagrams used herein are the three diagram fragments shown in Fig. 1. The green lines in the diagrams in the figure denote particle (upwards pointing) and hole (downwards pointing) lines, respectively. The red wiggly lines in the diagrams represent a virtual photon line describing

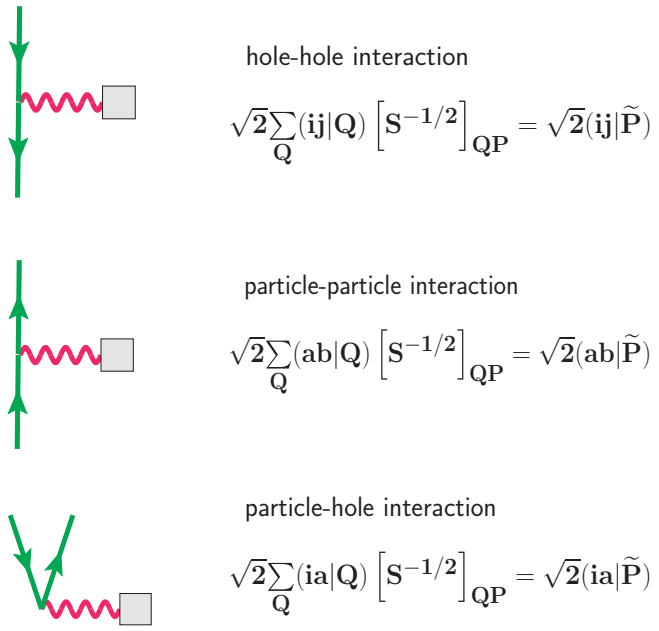

FIG. 1. Relation between diagram fragments and algebraic expressions. Top: hole-hole integral; middle: particle-particle integral; bottom: particle-hole integral.

the interaction of the particle or hole with an unspecified perturbation, as marked by the grey boxes in the diagrams. In the corresponding algebraic expressions $(ia|P)$ denotes a three-index Coulomb repulsion integral between the density of the orbital product $\phi_i(\mathbf{r})\phi_a(\mathbf{r})$ (i: occupied; a: virtual) and an auxiliary function $g_P(\mathbf{r})$. The operation of the inverse of the square-root Coulomb metric of the auxiliary function space transforms the functions into an orthonormal function set within the Coulomb norm; see, e.g., Refs. [75,76]. Due to this, any diagram containing the general auxiliary function space vertex can be contracted with another diagram containing this vertex to obtain the final self-energy contributions. As an example, the two-electron Coulomb-repulsion integral $(ia|jb)$ (chemist's notation) can be obtained by the contraction of the particle-hole (ph) diagrams of Fig. 1:

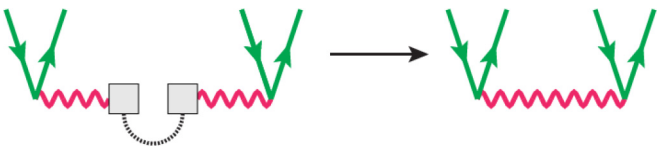

(9)

Finally, the factor of $\sqrt{2}$ appearing in the algebraic expressions in Fig. 1 is a spin factor since only closed-shell systems shall be considered.

The zeroth- and first-order contributions to the self-energy [i.e., the Hartree-Fock orbital energies in Eq. (8)] are given by the three diagrams [28,77]

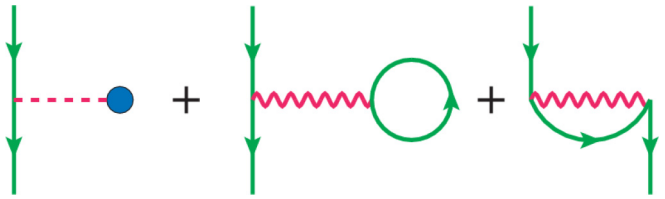

(10)

Here the blue vertex in the first diagram denotes the external potential of the nuclei, the second diagram represents a Coulomb interaction to first order, and the third diagram is an exchange diagram to first order and originates from the antisymmetry condition on the wave function. Note that from now on only the hole-hole part to $\mathbf{\Sigma}(\omega)$ will be considered. The corresponding particle-particle contributions can be obtained in a completely analogous way by swapping the directions of the outer fermion lines.

Regarding the rules to translate the (Goldstone-type) diagram expressions back into algebraic expressions, including sign and prefactor rules, refer to Refs. [6,16,27,77–80].

2. *Correlation contribution to the self-energy*

The first correlation correction to Koopman's theorem is given by the term [27]

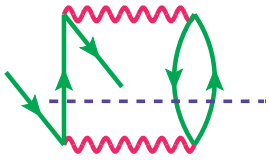

$$\Sigma^{\mathrm{corr}}_{\mathrm{pq}}(\omega) = -2\sum_{\mathrm{i,a,b}}\frac{(\mathrm{pa}|\mathrm{jb})(\mathrm{jb}|\mathrm{aq})}{\omega+\varepsilon_{\mathrm{j}}-\varepsilon_{\mathrm{a}}-\varepsilon_{\mathrm{b}}}$$

(11)

where the blue dotted line is added in order to indicate that an energy denominator with energy levels corresponding to the intersections with the fermion lines has to be added in the algebraic term, see, e.g., Ref. [77]. This contribution can be interpreted as a correlation term because the electron entering in a hole state is excited into an unoccupied state when interacting with the many-body system, producing a particle-hole pair. In the second interaction in the diagram in Eq. (11) the electron interacts again with the ph pair and scatters back into a hole state.

Note that in the case of the insertion of $\omega = \varepsilon_i$ into the diagram in Eq. (11), according to a first iteration of Eq. (7), the bottom fragment of the diagram may be rewritten as

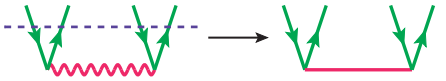

$$\frac{2(\mathrm{ia}|\mathrm{jb})}{\varepsilon_{\mathrm{i}}+\varepsilon_{\mathrm{j}}-\varepsilon_{\mathrm{a}}-\varepsilon_{\mathrm{b}}}$$

(12)

which actually corresponds to the direct part to the double amplitudes within second-order Møller-Plesset perturbation (MP2) theory. The second-order correlation contribution to the self-energy can therefore be transformed to the RPA one by replacing the MP2 amplitudes by the RPA amplitudes in Eq. (11). These can be obtained by iterating the Riccati-type

equation [77,81,82]:

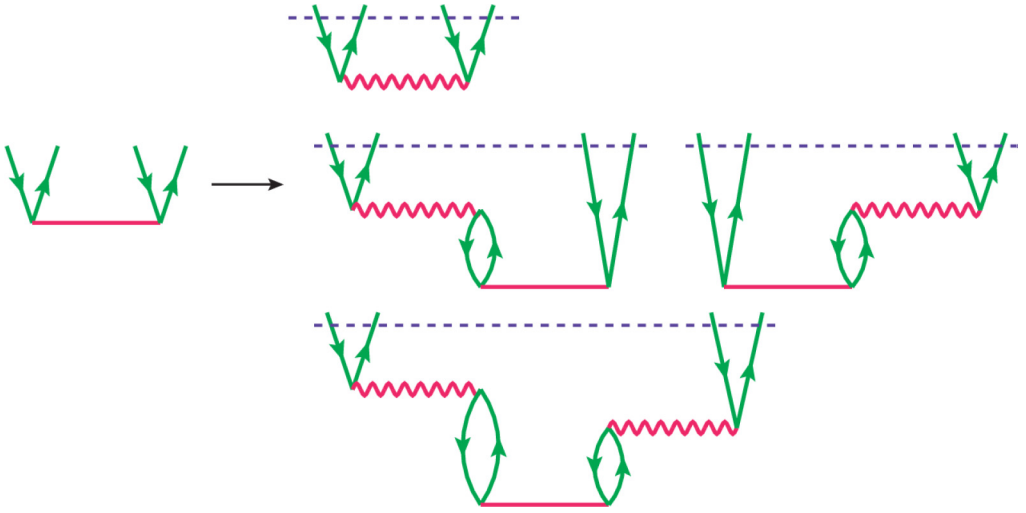

(13)

In Eq. (13), the initial amplitudes have to be inserted into the three diagrams in the middle and bottom on the right-hand side. The sum of these plus the first-order doubles contribution then yield a new approximation to the amplitudes. The repeated iteration of the equation leads, after a contraction with two-electron integrals, to all direct ring diagrams and thus defines the RPA doubles amplitudes.

It was shown in Ref. [59] that a computational efficient algorithm to compute the RPA amplitudes can be derived if not iterating the full amplitudes themselves, but by iterating the contraction of the amplitudes with the ph-diagram of Fig. 1 instead. The first iteration of this method reads

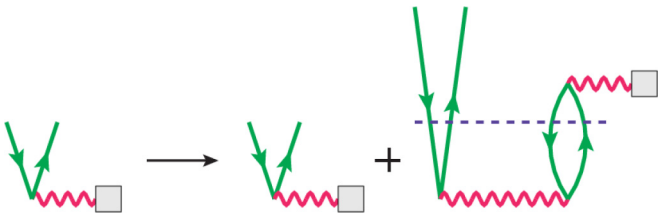

(14)

The construction of the second term in Eq. (14) can be decomposed into two steps: In the first step the doubles amplitudes are calculated from the two ph diagrams of Fig. 1. In the second step the amplitudes are then contracted again with the ph fragment of the figure so that a screened interaction correction to the bare ph diagrams is obtained. With this the iterative method of Ref. [59] can be written as

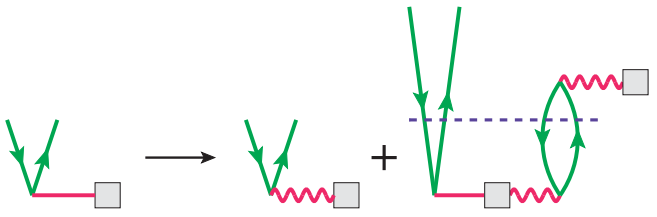

(15)

where the ph fragment containing the solid red line now is the actual quantity that is iterated.

It was shown in Refs. [70,83,84] that the direct RPA (used in conjunction with a Kohn-Sham reference determinant) is not very accurate in describing electron correlation energies of molecules. The reason for this mainly originates from the fact that the RPA contains many exclusion-principle violating (EPV) diagrams in each order of perturbation theory which are not canceled by corresponding exchange-diagram counterparts, leading to a large overestimation of electron correlation energies [77]. This deviation of the RPA correlation energies from accurate correlation energies is also termed as a self-correlation error and can be viewed as a generalization of the self-interaction error of the Hartree method in first order.

In order to correct this error of the RPA, the doubles amplitudes have to be antisymmetrized according to

(16)

If this antisymmetrization step is applied to the converged RPA amplitudes of the iterative method described above, then the contraction of the amplitudes with the two-electron integrals yield the correlation energy within the so-called SOSEX (second-order screened exchange) method by Kresse *et al.* [85]. While with this the EPV diagrams appearing in the perturbation series expansion of the RPA correlation energy are canceled in each order, the resulting SOSEX correlation energy is incomplete with respect to ph-interaction terms already in third order. In Ref. [59] therefore an alternative method has been derived which yields all ph-interaction diagrams in a perturbation expansion. This is achieved by applying the antisymmetrization of the doubles amplitudes in each iteration of the amplitude update step. Using the auxiliary basis set representation of the general interaction vertex, the recursion relation for the ph interaction in the RPAX2 method

reads

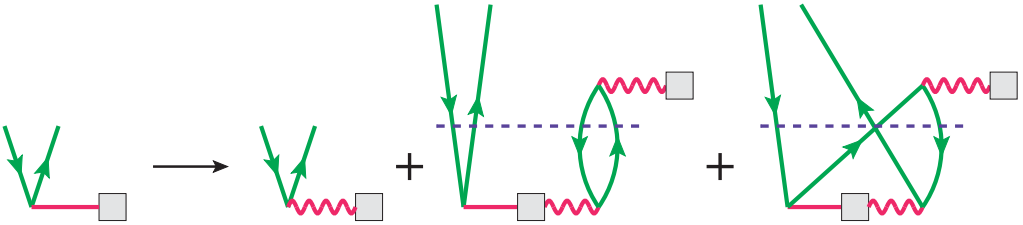

(17)

An insertion of the converged RPAX2 doubles amplitudes into the self-energy diagram

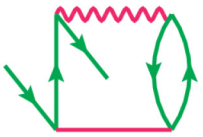

(18)

yields correlation energy corrections to the occupied single-particle states on the RPAX2 level. Note that the sum of these corrections over all occupied states yields the RPAX2 correlation energy of the N-particle system. It can thus be followed that the correlation contribution to $\mathbf{\Sigma}(\omega)$ leads to a stabilization of the N-particle system relative to the $(N-1)$-particle system and therefore is always a positive contribution to the ionization energy [27,31]. In the case of electron affinities an analoguous behavior exists that leads to a positive self-energy shift (reduction of the EA) since again the N-particle system is favored compared to the $(N+1)$ system due to the correlation contribution.

3. Relaxation contribution to the self-energy

The first relaxation correction to Koopman's theorem again occurs in second order and is given by the term

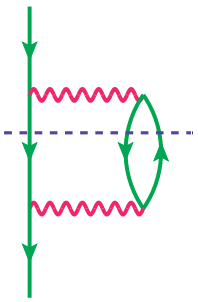

$$\Sigma^{\mathrm{relax}}_{\mathbf{pq}}(\omega) = -\mathbf{2}\sum_{\mathbf{i,j,b}}\frac{(\mathbf{pi}|\mathbf{jb})(\mathbf{jb}|\mathbf{iq})}{\varepsilon_{\mathbf{i}}+\varepsilon_{\mathbf{j}}-\omega-\varepsilon_{\mathbf{b}}} \tag{19}$$

In contrast to the correlation contribution, the electron entering in a hole state is scattered into another hole state upon interaction with the many-body system. Again this process is accompanied with the excitation of an electron in an occupied state into an unoccupied state (leading to a particle-hole pair). The whole interaction therefore defines a double excitation of the form

$$\begin{aligned} i &\rightarrow j, \\ k &\rightarrow a, \end{aligned}$$

which occurs in the second-order energy of the $(N-1)$ system. Such excitations are absent in the N-particle system because j is an occupied state [27]. Because of this, the relaxation contribution always lowers the energy of the $(N-1)$ system [$(N+1)$ system] as compared to the N-particle system and is thus a negative (positive) contribution to the ionization energy (electron affinity). Note that the relaxation contribution can be further split into an orbital-relaxation term and a pair-relaxation term by separating the self-energy expression into a single- and double-excitation part [27,31]. In this work no such differentiation will be made.

The question is now how the self-energy diagram of Eq. (19) can be expanded within the RPA? Making use of the techniques derived in Sec. II B 2, the following recursive procedure can be applied to obtain all time-forward ring-diagram contributions:

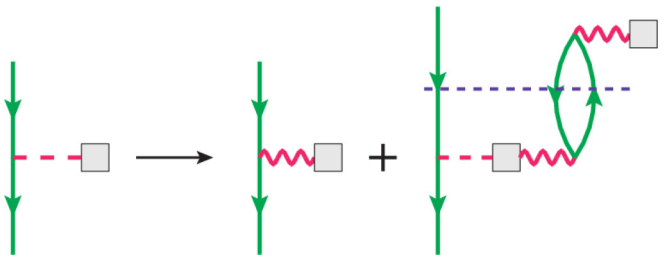

(20)

with the dashed vertex line now denoting the interaction of the hole-hole pair with the many-body system. The repeated iteration of the above equation produces (omitting the horizontal energy denominator lines)

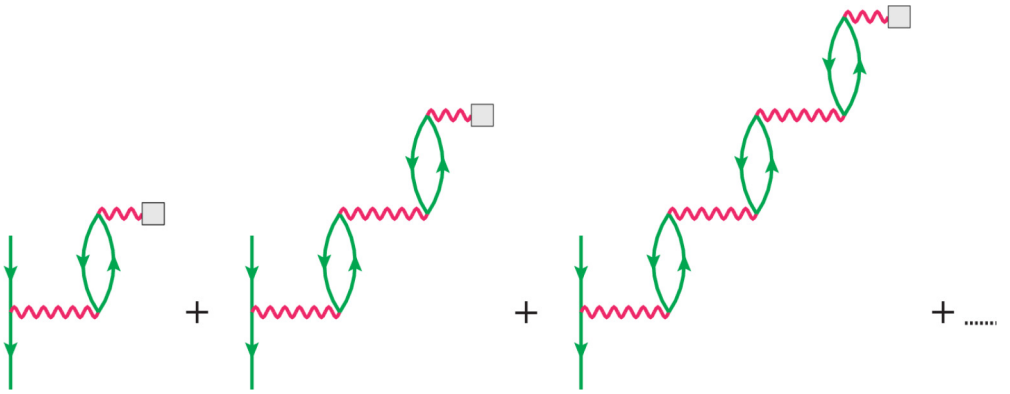

(21)

A contraction with the hole-hole (hh) diagram of Fig. 1 then yields the self-energy terms

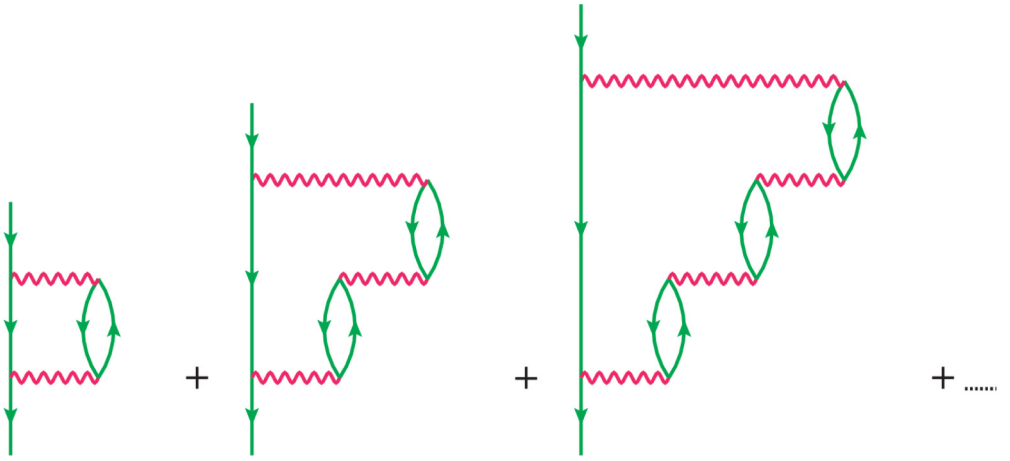

(22)

Note, however, that this series misses ring diagram contributions containing energy independent fragments. These are those diagrams which possess factorized energy denominator terms that exclude the energy ω; see also the Supplemental Material [74]. The first such contribution occurs in third order and is given by

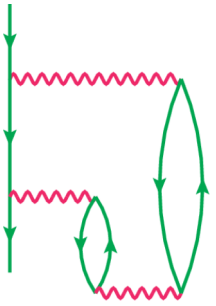

(23)

To take these missing ring diagrams into account, the iterative equation above is slightly modified to

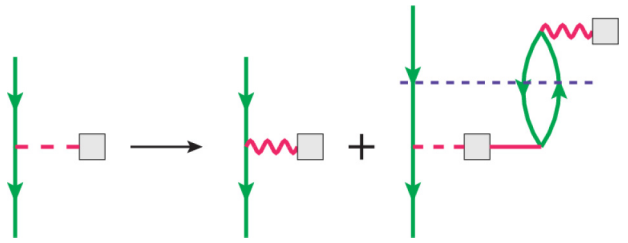

(24)

i.e., the hh-interaction fragment is now contracted with the solutions to the RPA doubles amplitude equation (15) instead of the bare ph interaction [as is indicated by the solid red line in Eq. (24)]. As an example, the insertion of the first-order solution to Eq. (15), i.e., Eq. (14), into Eq. (24) gives

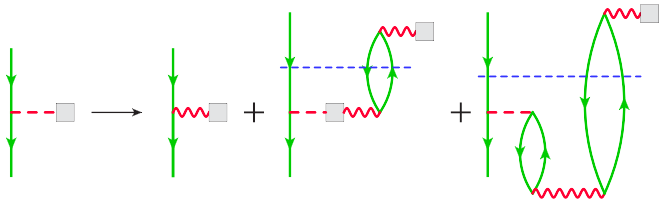

(25)

Finally, exchange interaction contributions to the relaxation part of the self-energy can be obtained in an analogous way as described for the correlation part; see Sec. II B 2. The modified recursion relation for the RPAX2 hh interaction then reads

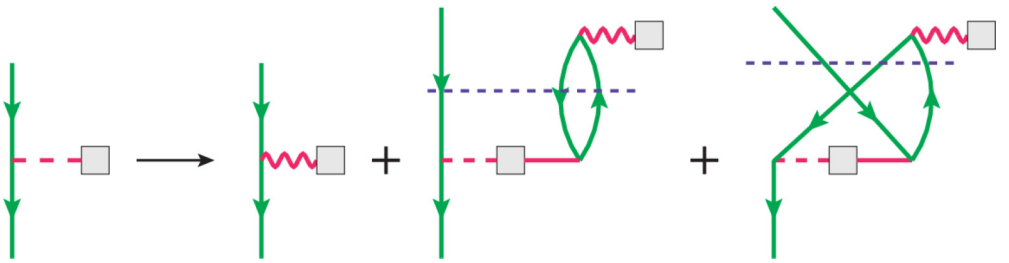

(26)

Note that here the solutions to the RPA ph-interaction diagrams are replaced with the corresponding solutions to the RPAX2 ph interactions. Analogous to the RPAX2 amplitude equation (17) it can be verified that the iterative procedure defined by Eq. (26) requires at most contractions which scale as $\mathcal{N}^5$ with respect to the molecular size $\mathcal{N}$. Due to this, the combined approach for calculating self-energy contributions described in Sec. II B 2 and in this section is not much more computationally demanding than computational schemes for second-order methods.

4. Static self-energy contributions

In third and higher orders of the perturbation theory expansion of the self-energy also terms which are independent of the energy occur. The leading-order terms of the static part of the self-energy are given by [6,13,86]

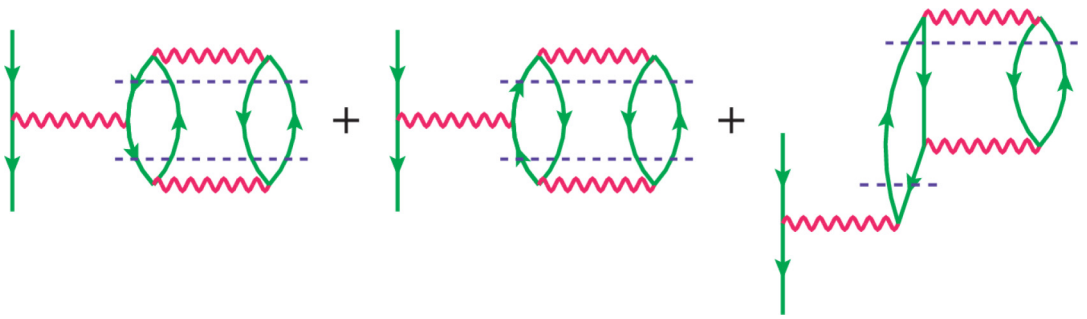

(27)

Note that a fourth diagram exists which can be obtained by a 180° rotation of the third one around either of the two denominator lines and a swapping of all directions of the fermion lines. This contribution, however, is identical to the third one if only the diagonal part to $\mathbf{\Sigma}(\omega)$ is considered and can be taken into account by a prefactor of 2 added to the diagram. As one may observe from the forms of the static self-energy diagrams in Eq. (27), they describe the interactions of an extra electron with the occupied-occupied (first term), virtual-virtual (second term), and occupied-virtual (third term) part of an effective single-particle

correlation potential of the many-body system. In fact, the correlation potential corrections to the HF potential appearing in the diagrams above will also have to be considered if off-diagonal elements of $\mathbf{\Sigma}(\omega)$ are taken into account, leading to single-particle equations which define Brueckner orbitals if ω is replaced by the corresponding orbital energies; see also Refs. [39,41,73,87–89].

The third-order terms of the static self-energy in Eq. (27) can easily be generalized to the RPA upon an insertion of the RPA amplitudes for all second-order doubles amplitude fragments, leading to

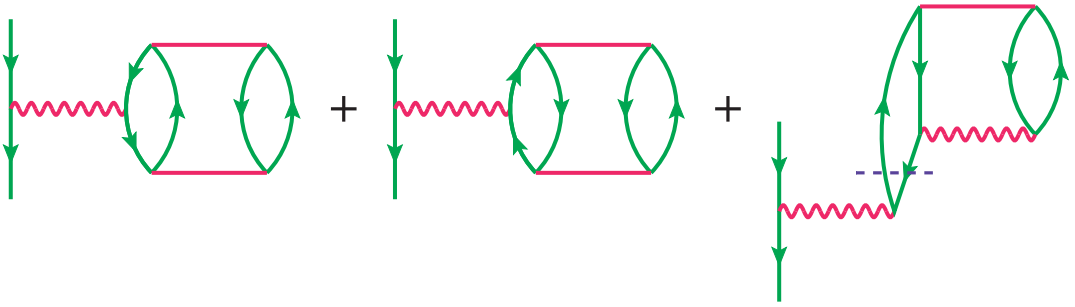

(28)

Again, the corresponding static self-energy contributions of the RPAX2 method can be obtained by replacing the RPA double amplitudes by the RPAX2 amplitudes as described in Sec. II B 2.

III. COMPUTATIONAL DETAILS

The Green's-function methods employing RPA and RPAX2 self-energy contributions as described in Secs. II B 2, II B 3, and II B 4 have been used to compute the occupied and lowest unoccupied energy levels of the molecules from the GW27 database [53]. The original structures of the molecules of this database have been taken from the Turbomole database [90] which was generated by using geometry optimizations employing the Becke-Perdew Kohn-Sham energy functional [91,92] and using small basis sets. Because of this, all the structures of the GW27 set have been reoptimized with MP2 using the cc-pVTZ basis set by Dunning and co-workers [93–96] (except Cs_2, Au_2, and Au_4: def2-TZVP basis set with additional effective core potential functions [97,98]). It was then verified that total CCSD(T) (coupled-cluster singles and doubles with perturbative triples) energies are lower throughout if using the reoptimized structures instead of the original ones. It should be noted that the geometric alternation also leads to partially significant changes in the CCSD(T) ionization energies, most notably for H_2 ($\sim +0.2$ eV) and F_2($\sim +0.3$ eV). Since not all molecules of the GW27 database build a stabilized anion (relative to the neutral system), only those molecules for which the vertical CCSD(T) EAs are positive are used for benchmarking the propagator methods.

To enable a comparison with experimental measurements, which often [99] provide only estimates for the adiabatic ionization potentials and electron affinities, also the cations and anions for the molecules from the GW27 database have been optimized on the MP2 level using the cc-pVTZ basis sets. For all optimized structures the zero-point vibrational energies have then been calculated with MP2. The only exception to this were the neutral and charged anthracene and naphthacene molecules. Here the vibrational frequencies were calculated with the B3LYP KS energy functional [91,100,101] using the geometries optimized with this method (employing the cc-pVTZ basis set by Dunning [93–96]). The structure optimizations and frequency calculations have been performed using the GAUSSIAN09 program [102]. All structures and adiabatic energy corrections to the ionization potentials and electron affinities are compiled in the Supplemental Material to this work [74].

For comparison, the IPs and EAs have also been computed with the standard *ab initio* methods HF, MP2, CCSD, and CCSD(T) using the MOLPRO program [103,104]. Here always a spin-restricted open-shell configuration of the reference state was used in the correlation energy calculations. In addition, RPA and RPAX2 total-energy calculations were performed using the approach described in Ref. [59]. In the case of the charged molecules, in these calculations a spin-unrestricted approach was used. Note that in contrast to previous works [59,60,105] here the Hartree-Fock determinant has always been chosen as reference determinant in the RPA and RPAX2 calculations.

In order to investigate the approximations used in the calculations of the self-energy contributions described in Sec. II A, the second- and third-order outer-valence Green's function (OVGF) method by Ortiz has been used to compute the IPs and EAs, too [13,15,17,18,35]. For this, in the case of the third-order calculations the P3 approximation by Ortiz has been utilized; see Ref. [36]. These calculations were done with the GAUSSIAN09 program [102].

In all energy difference and propagator calculations the aug-cc-pVTZ and aug-cc-pVQZ basis sets by Dunning *et al.* [93–96] have been utilized, except for Cs_2, Au_2, and Au_4 where the def2-TZVP and def2-QZVP basis sets [97,98,106] were employed. In the case of the energy difference methods the resulting correlation energies have then been extrapolated to the complete basis set limit (cbs) using the two-point extrapolation scheme by Bak *et al.* [107]. The only exceptions to this were the CCSD and CCSD(T) correlation energies of the anthracene and naphthacene molecule. Here the complete basis set limit was estimated by adding the ΔCCSD(T) correction to the extrapolated MP2 correlation energy [108,109]. For the anthracene molecule this correction has been calculated with the aug-cc-pVTZ basis set and for the naphthacene molecule the aug-cc-pVDZ basis set was used for calculating the ΔCCSD(T) term. The cbs results for the reference energy contributions were not obtained by corresponding basis set

TABLE I. Basis set dependence of the correlation, relaxation, and static self-energy contribution to the ionization energy of the RPAX2-GF method for the H_2O molecule (in eV).

Basis set	$\Sigma^{\mathrm{RPAX2}}_{\mathrm{corr}}$	$\Sigma^{\mathrm{RPAX2}}_{\mathrm{relx}}$	$\Sigma^{\mathrm{RPAX2}}_{\mathrm{static}}$
aVDZ	−1.251	2.754	−0.443
aVTZ	−1.580	2.831	−0.129
aVQZ	−1.705	2.841	−0.009
aV5Z	−1.756	2.843	0.043
aV6Z	−1.779	2.843	0.065

extrapolation techniques but were estimated using the largest basis set (aug-cc-pVQZ) used.

In the case of the Green's-function methods of this work a basis set extrapolation was only applied to the correlation contribution to the self-energy while the relaxation and static contributions were estimated by the results obtained with the aug-cc-pVQZ basis set to estimate the complete basis set limit of the IPs and EAs. In the case of the relaxation energy contribution to the IP it was found that this quantity is almost converged with this basis set; see Table I which shows the basis set convergence of the different contributions to the self-energy for the water molecule. In contrast to this, as can be seen in Table I, the static self-energy contribution changes significantly and even switches its sign upon an increase of the basis set. However, for most of the molecules studied in this work the static self-energy contribution is fairly small in magnitude, see Table I and the Supplemental Material [74], and therefore it can be expected that a basis set extrapolation would not alter the cbs estimates significantly.

In order to accelerate the convergence behavior of the iterative equations (17) and (26) for the amplitudes, the damping method described in Ref. [59] has been utilized. Note also that in the case of low-lying occupied and higher virtual energy states a convergence of Eq. (26) for the amplitudes of the relaxation contribution is often hampered due to an intruder state problem (see also Refs. [32,73] where this problem is discussed). In such cases a damping shift of 0.1 hartree was added to the energy denominators to enable a convergence of the iterative solution method. The results presented in this work, however, were all obtained without requiring this damping approach.

For the auxiliary function space used in the RPA-GF calculations (see Fig. 1) the corresponding aug-cc-pVTZ/QZ-MP2Fit density-fitting basis sets by Weigend [110] have been utilized (except Cs_2, Au_2, and Au_4: def2-TZVP-MP2Fit fitting basis set [111]).

Core electrons were kept frozen in all correlation energy calculations.

TABLE II. Ionization energies: comparison between adiabatically corrected CCSD(T) energies to experimental results (eV). Experimental methods: PE: photoelectron spectroscopy; S: optical spectroscopy; PI: photoionization mass spectrometry; TE: threshold electron detection; LS: laser spectroscopy; EI: electron impact.

	CCSD(T)			CCSD(T)	Experiment		
Molecule	Vertical	$\Delta E^{\mathrm{deform}}$	ΔZPE	Adiabatic		Method	Reference
H_2	16.479	−0.921	−0.135	15.423	15.425927	PE	[112]
Li_2	5.188	−0.082	−0.021	5.085	5.1127 ±0.0003	S	[113]
Na_2	4.815	−0.109	−0.010	4.696	4.8951 ±0.0002	PI	[114]
Cs_2	3.411	−0.195	−0.001	3.215	3.7 ± 0.1	PI	[114]
F_2	15.922	−0.005	−0.009	15.908	15.697 ±0.003	PE	[115]
N_2	15.613	−0.046	−0.006	15.561	15.581 ±0.008	S	[116]
BF	11.200	−0.081	0.018	11.137	11.12 ±0.01	PE	[117]
LiH	8.006	−0.297	−0.019	7.690	7.9±0.3	EI	[144]
CO_2	13.914	−0.002	−0.154	13.758	13.778 ±0.002	PE	[118]
H_2O	12.793	−0.108	−0.068	12.617	12.6188 ±0.0009	PI	[119]
NH_3	11.036	−0.807	−0.042	10.187	10.186	TE	[120]
SiH_4	12.870	−1.363	−0.161	11.346	11.2 ±0.1	PI	[121]
SF_4	12.990	−0.994	0.039	12.035	12.08 ±0.10	EI	[122]
Au_2	9.412	−0.119	−0.003	9.290	9.5 ±0.3	EI	[123]
Au_4	7.894	−0.017	−0.002	7.875			
CH_4	14.561	−1.529	−0.285	12.747	12.75 ±0.02	PE	[124]
C_2H_6	12.789	−1.053	−0.175	11.561	11.56 ±0.02	EI	[125]
C_3H_8	12.205	−0.936	−0.237	11.032	11.01 ±0.07	EI	[126]
C_4H_{10}	11.942	−0.665	0.092	11.369	10.87 ±0.05	EI	[127]
iso-C_4H_{10}	11.835	−0.858	−0.339	10.638	10.74 ±0.05	EI	[127]
C_2H_4	10.741	−0.175	−0.058	10.508	10.5138 ±0.0006	LS	[128]
acetone	9.904	−0.103	−0.045	9.756	9.694 ±0.006	PI	[129]
acrolein	10.304	0.074	0.004	10.382	10.11	PE	[130]
C_6H_6	9.471	−0.132	−0.059	9.280	9.24384 ±0.00006	TE	[131]
naphthalene	8.258	−0.069	0.342	8.531	8.1442 ±0.0009	TE	[132]
anthracene	7.482	−0.046	0.016	7.452	7.439 ±0.006	LS	[133]
naphthacene	6.964	−0.042	0.028	6.950	6.97	EI	[134]

TABLE III. Electron affinities: comparison between adiabatically corrected CCSD(T) energies to experimental results (eV). Experimental methods: LPES: laser photoelectron spectroscopy; CIDC: kinetic method; NBIE: neutral beam ionization potentials; IMRB: ion or molecule reaction bracketing.

	CCSD(T)			CCSD(T)	Experiment		
Molecule	Vertical	ΔE^{deform}	ΔZPE	Adiabatic		Method	Reference
Na_2	0.387	0.058	0.004	0.449	0.430 ± 0.015	LPES	[135]
Cs_2	0.358	0.084	0.001	0.443	0.469 ± 0.015	LPES	[135]
F_2	0.187	2.958	0.033	3.178	3.120 ± 0.070	CIDC	[136]
LiH	0.296	0.015	0.017	0.328	0.342 ± 0.012	LPES	[137]
CO_2	−0.820	0.161	0.078	−0.581	-0.60 ± 0.20	NBIE	[145]
SF_4	−0.253	1.451	0.082	1.280	1.50 ± 0.20	IMRB	[138]
Au_2	1.677	0.083	0.003	1.763	1.940 ± 0.020	LPES	[139]
Au_4	2.246	−0.074	−0.012	2.160	2.692 ± 0.030	LPES	[140]
naphthalene	−0.443	0.107	0.012	−0.324	-0.200 ± 0.050	LPES	[141]
anthracene	0.359	0.077	0.144	0.580	0.530 ± 0.020	LPES	[142]
naphthacene	0.928	0.069	0.126	1.123	1.0580 ± 0.0050	LPES	[142]

IV. RESULTS

A. Reference values

Ionization potentials (IPs) and electron affinities (EAs) can be obtained with high accuracy from experimental measurements, e.g., photoelectron spectroscopy, electron impact experiments, or photoionization mass spectrometry. In addition, the measured values usually correspond to the adiabatic IPs and EAs rather than the vertical ones. Because of this, a direct comparison between the results from the electron propagator calculations and the experimental values is not possible since the deformation energies, stemming from the relaxation of the molecular structures after ionization or electron attachment, as well as the differences in the zero-point vibrational energies of the neutral and charged systems, can be quite large; see Tables II and III.

Because of this, in this work the results for the RPA Green's-function (GF) methods will be compared to vertical CCSD(T) IPs and EAs. These values are compiled in the corresponding second columns in Tables II and III. Note that corresponding coupled-cluster results for the ionization energies of the GW27 molecules have also recently been presented by Klopper *et al.* [143]. Here, however, the geometries of the original GW27 database were used in the calculations (see discussion in Sec. III) and the results have not been extrapolated to the complete basis set limit but were calculated using the def2-TZVP basis set.

In order to assess the accuracy of the CCSD(T) reference values, they have been corrected by the deformation and zero-point vibrational energy contributions calculated using the MP2 method with triple-ζ quality basis sets; see Tables II and III. We believe that this is a consistent approach, since the MP2 method was also used to optimize the structures of the neutral and charged molecules. Moreover, note that vibrational frequency calculations using the CCSD(T) method are not feasible anymore for all but the smallest systems of the GW27 database. The corresponding corrected IPs and EAs are listed in the fifth columns in Tables II and III.

For comparison, the sixth columns in Tables II and III show experimental results for the IPs and EAs that have been collected from the web book of chemistry [144]. In the case of the ionization energies, Table II, it can be observed that the adiabatic coupled-cluster estimates are in a very good agreement with the experimental results. In most cases the differences between the CCSD(T) values and the experimental IPs are not larger than ±0.1 eV. The only notable exceptions to this are the butane molecule and the naphthalene molecule where deviations of +0.5 and +0.35 eV are observed, respectively. Note also that in a few cases, e.g., LiH or Au_2, the deviations are of the order of 0.2 eV which lies, however, in the range of the experimental uncertainty of the experimental measurement (±0.3 eV both, in the case of LiH and Au_2 using electron impact experiments).

Table III shows, where available, also a comparison between the adiabatic CCSD(T) EAs to experimental values. With only two exceptions, CO_2 and naphthalene, the experimental affinity values are positive, indicating a stable anion relative to the neutral molecule. In most cases a fairly good agreement between the CCSD(T) results and the experiment is found; see Table III. One of the most striking example that shows the importance of the inclusion of the deformation energies in the theoretical estimates is found for the SF_4 molecule. Here the EA changes from −0.25 eV for the vertical case to +1.28 eV due to the relaxation of the anion. The latter value compares quite well with the experimental number of 1.50 ± 0.20 eV; see Table III. The largest deviation between the CCSD(T) estimates and the experiment is found for the gold tetramer where the experimental number differs by more than 0.5 eV from the theoretical result. In all other cases the differences between theory and experiment are within a range of ±0.2 eV (note in this context that the web book website [144] lists a value of -1.6 ± 0.1 eV for the EA of CO_2 for the corresponding reference by Compton *et al.* [145]; this apparently is an error, since the original source gives an estimate of -0.6 ± 0.2 eV for this molecule; an error report has been sent to the National Institute of Standards and Technology).

In summary, it has been proven that the adiabatically corrected CCSD(T) IPs and EAs are in fairly good agreement with experimental measurements. Accordingly, the corresponding vertical CCSD(T) values will serve well as a reference for

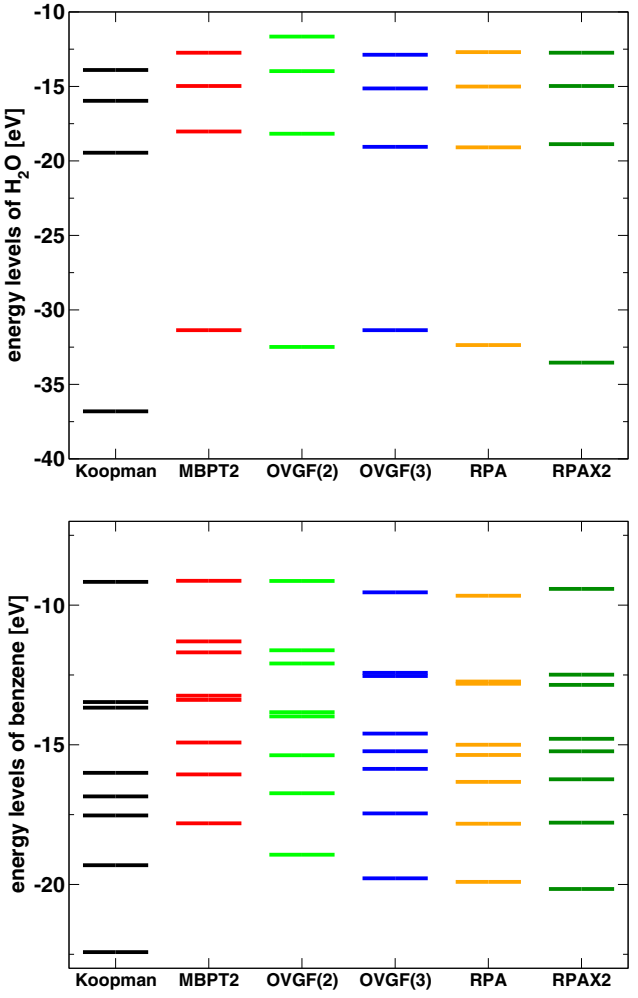

FIG. 2. Comparison of the highest occupied energy levels of H_2O (top) and benzene (bottom) for the different propagator methods (aug-cc-pVQZ basis set).

assessing the accuracy of the more approximate Green's-function methods considered in this work.

B. Quasiparticle energy levels

The influence of the different approximations to the self-energy corrections to Koopman's theorem is shown in Fig. 2 for the highest occupied energy levels of the H_2O (top) and benzene molecule (bottom), respectively. As can be seen in the diagrams in the figure, for all Green's-function (GF) methods the largest corrections to Koopman's theorem are obtained for the lower energy levels in both cases, while for the highest occupied molecular orbital (HOMO) energies the Koopman's theorem results agree better with the OVGF and RPA results. The reason for this can be attributed to the much larger relaxation contribution if an electron is removed from a low-lying state as compared to the removal from the outer valence energy levels. It can also be seen that the relaxation contribution usually dominates the correlation contribution to the self-energy, since most of the energy levels from the Green's-function methods are shifted upwards compared to Koopman's theorem; see also below.

A comparison between the levels for the two second-order methods MBPT2 and OVGF(2) highlights the influence of the diagonal and non-self-consistent approximations on the energy levels (see Sec. II A) applied in the MBPT2 calculations. One can observe that the effect of this approximation is nonuniform for the two molecules considered in the figure. In the case of the H_2O molecule it leads to a downward shift of the highest quasiparticle energies compared to the OVGF(2) method while in the case of the benzene molecule a reverse trend is observed. Note, however, that in this case both the highest level of the MBPT2 method and the OVGF(2) method are almost identical to the Koopman's theorem value, i.e., here a strong cancellation of the correlation and relaxation self-energy contributions occurs; see also Supplemental Material [74].

The energy levels from the RPA and RPAX2 methods are very similar for the highest levels while in the case of the lower-lying energy levels the RPAX2 energies are slightly lower than the RPA ones; see Fig. 2. It can be seen in the diagrams in the figure that both the RPA and RPAX2 quasiparticle energies are closer to the third-order OVGF(3) energies than the energies from both second-order approaches. This indicates that the

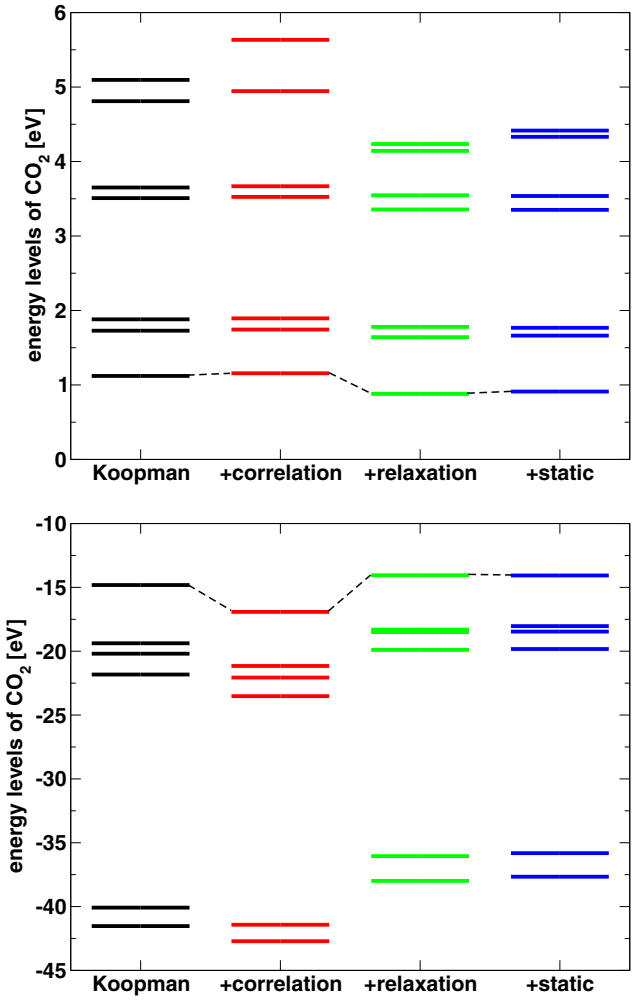

FIG. 3. CO_2 molecule: influence of the correlation, relaxation, and static contributions to the self-energy on the energy levels (RPAX2, aug-cc-pVQZ basis set). Top: lowest unoccupied levels; bottom: occupied levels.

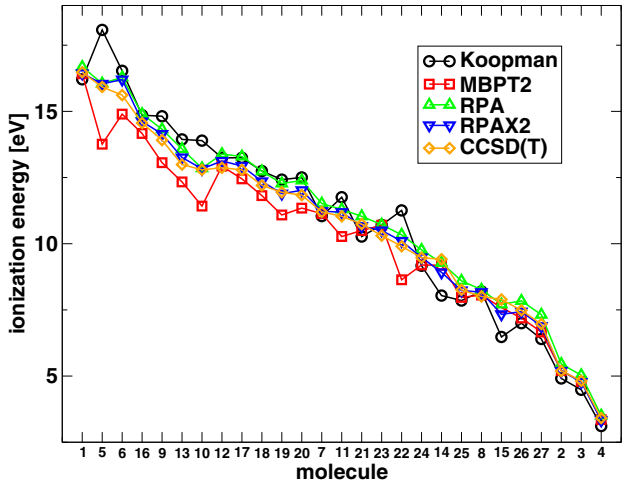

FIG. 4. Ionization energies for the GW27 molecules. The molecules are ordered according to the magnitude of the CCSD(T) energies. See Table IV for labeling of the molecules.

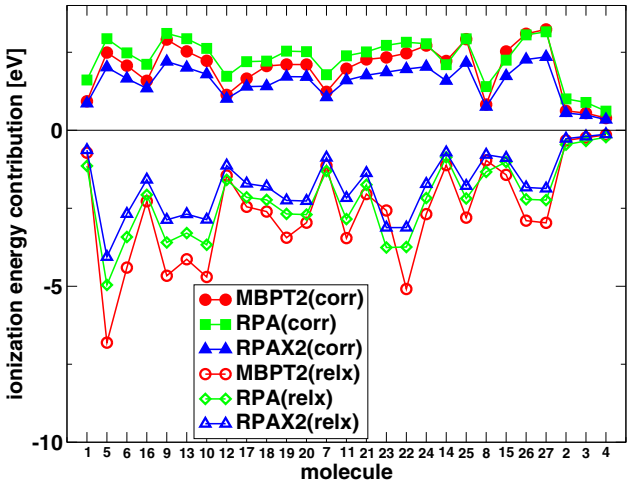

FIG. 5. Correlation and relaxation energy contributions to the ionization energies of the GW27 molecules. The molecules are ordered according to the magnitude of the CCSD(T) energies. See Table IV for labeling of the molecules.

common third-order contributions to the self-energy of the three methods are mainly responsible for the differences to the second-order self-energy levels. Furthermore, it may be that the diagonal and non-self-consistent approximations applied in the RPA and RPAX2 approaches have a smaller influence on the poles of the Green's function than at a second-order level. This has to be studied in a future work.

TABLE IV. Labeling of molecules of the GW27 database.

Molecule	Label
H_2	1
Li_2	2
Na_2	3
Cs_2	4
F_2	5
N_2	6
BF	7
LiH	8
CO_2	9
H_2O	10
NH_3	11
SiH_4	12
SF_4	13
Au_2	14
Au_4	15
CH_4	16
C_2H_6	17
C_3H_8	18
C_4H_{10}	19
iso-C_4H_{10}	20
C_2H_4	21
acetone	22
acrolein	23
C_6H_6	24
naphthalene	25
anthracene	26
naphthacene	27

In Fig. 3 the influence of the correlation, relaxation, and static contributions on the quasiparticle energies is shown for the occupied (bottom diagram) and lowest virtual (top diagram) energy levels of the CO_2 molecule. As has been explained in Sec. II B 2, the correlation contribution leads to an increase of the ionization energies (i.e., a downward shift of the occupied levels) and to a decrease of the electron affinities (corresponding to an upward shift of the energy levels). It can be seen in Fig. 3, however, that in the case of the occupied energy levels the correlation effect is much stronger than in the case of the lowest virtual energy levels for which only a very small correction to the Koopman's levels is found. In contrast to this, the relaxation contribution has a significant effect on the energy levels both for the occupied and virtual levels. Since it has an opposite effect on the magnitudes of the quasiparticle energies compared to

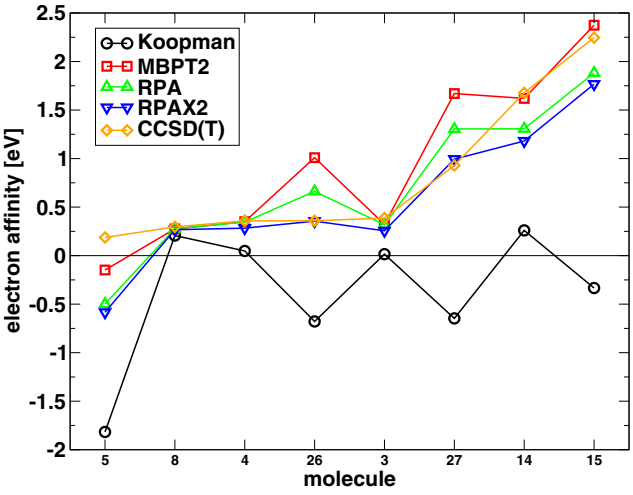

FIG. 6. Electron affinities for the GW27 molecules. The molecules are ordered according to the magnitude of the CCSD(T) energies. See Table IV for labeling of the molecules.

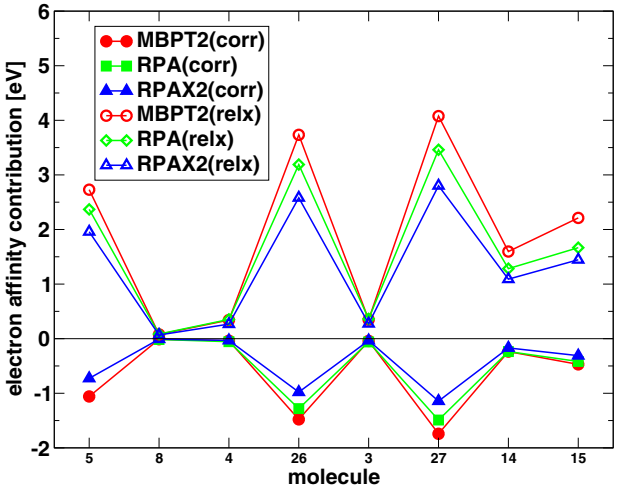

FIG. 7. Correlation and relaxation energy contributions to the electron affinities of the GW27 molecules. The molecules are ordered according to the magnitude of the CCSD(T) energies. See Table IV for labeling of the molecules.

the correlation contribution, the correlation and relaxation contributions strongly cancel each other for the occupied levels, but in the case of the unoccupied energy levels this cancellation is much smaller. A corresponding behavior was also found for all other systems of the GW27 benchmark set; see Supplemental Material to this work [74]. Finally, as can be seen in Fig. 3, the static contributions are very small compared to the correlation and relaxation counterparts. This, too, was found to be a common trend for all molecules considered in this work.

C. Comparison to reference values

The ionization energies and electron affinities for the GW27 sytems obtained with the different Green's-function methods are presented in Figs. 4 and 6 along with the vertical CCSD(T) values of Tables II and III. The ordering of the molecules plotted on the abscissa axis in the two diagrams has been done according to the magnitudes of the CCSD(T) IPs and EAs, respectively. The corresponding labels for the molecules used in the diagrams are given in Table IV.

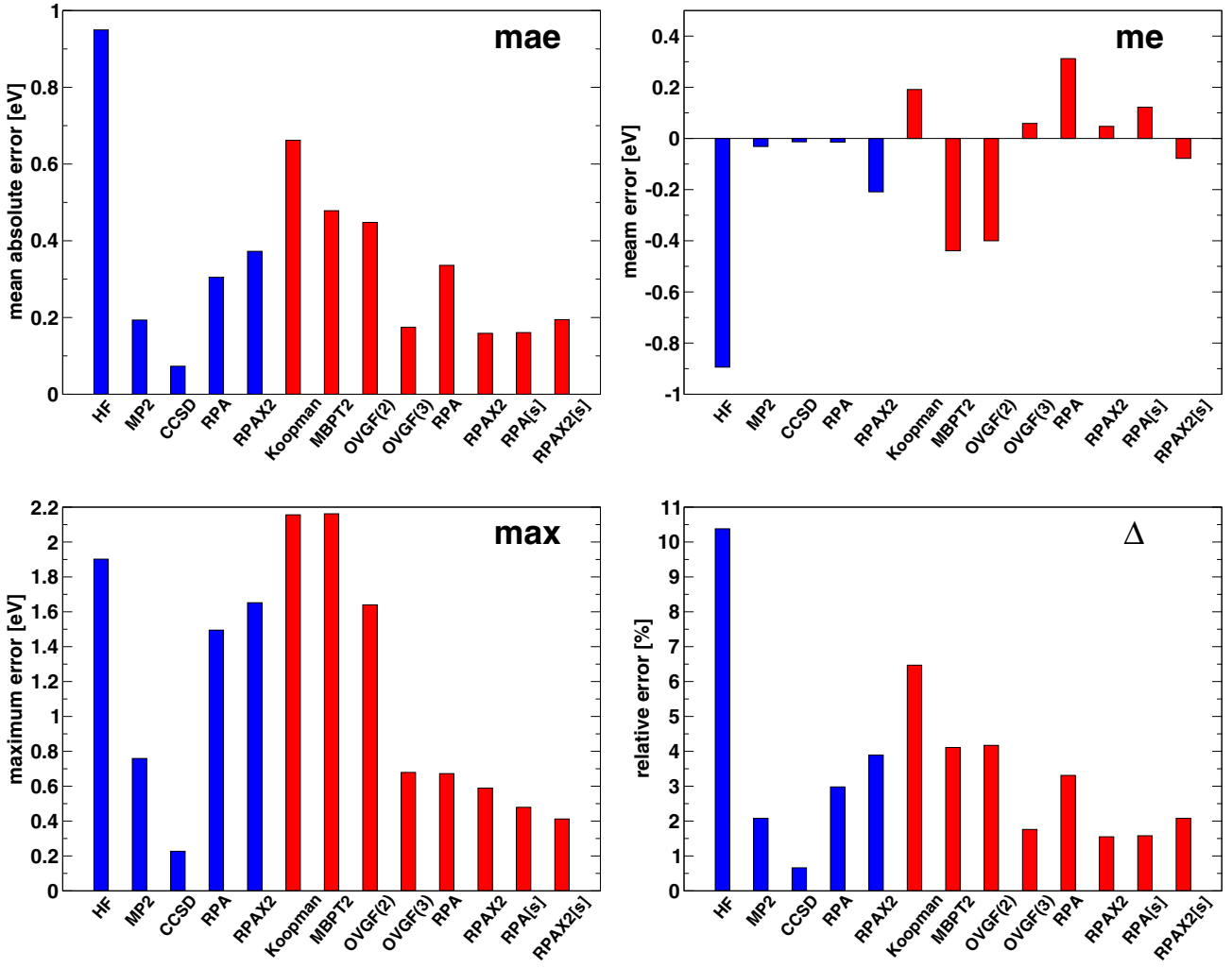

FIG. 8. Ionization energies: mean absolute errors (mae), mean errors (me), maximum errors (max), and relative errors (Δ) of the methods considered in this work to the CCSD(T) reference energies. Blue bars: energy difference approaches; red bars: Green's-function approaches. The notation [s] to the RPA and RPAX2 methods denotes additional static self-energy contributions taken into account.

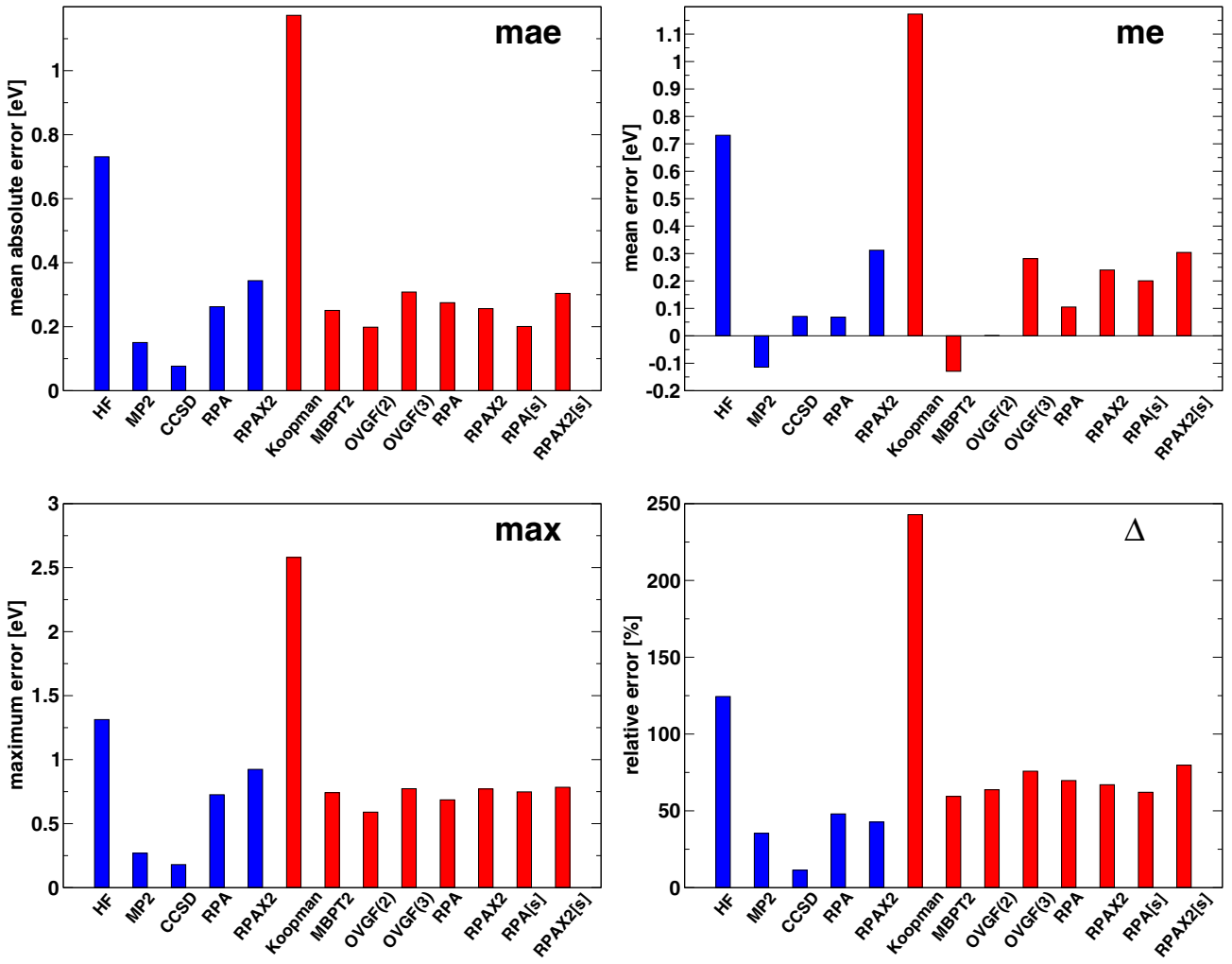

FIG. 9. Electron affinities: mean absolute errors (mae), mean errors (me), maximum errors (max), and relative errors (Δ) of the methods considered in this work to the CCSD(T) reference energies. Blue bars: energy difference approaches; red bars: Green's-function approaches. The notation [s] to the RPA and RPAX2 methods denotes additional static self-energy contributions taken into account.

In the case of the IPs, Fig. 4 shows that the MBPT2 values usually underestimate the CCSD(T) reference results for the systems where the magnitude of the ionization energy is large. A comparably large underestimation is observed for the F_2 (structure 5) and H_2O (structure 10) molecules. From the diagram in Fig. 5, which shows the correlation and relaxation contributions to the IPs, it can be seen that for these two molecules the correlation contribution to the self-energy, as obtained from the MBPT2 method, is quite large, explaining the deviations of the MBPT2 IPs from the reference values. In contrast to this, a significant improvement compared to the IPs at the second-order level is obtained by the RPA and RPAX2 methods; see Fig. 4. In Fig. 5 it can be seen that the differences observed between the MBPT2 IPs on the one hand and the RPA and RPAX2 IPs on the other hand mainly stem from a reduced correlation contribution, while the relaxation contributions are more similar for the different methods. A comparison between the RPA and RPAX2 correlation and relaxation contributions displayed in Fig. 5 shows that the RPA method yields larger values for these two in magnitude. These differences, however, strongly quench each other, leading to close IPs of the RPA and RPAX2 methods; see Fig. 4.

The electron affinities for the different methods are displayed in Fig. 6, again ordered according to the CCSD(T) reference values. One can observe that only a subset of the molecules from the GW27 database have a positive electron affinity, indicating a stabilization of the molecule upon an attachment of an electron. Molecules which belong to this class of systems are, e.g., the larger acene molecules, the F_2 molecule, and the gold dimer and tetramer. As is shown in Fig. 6, Koopman's theorem is unable to describe this stabilization effect. The reason for this is given by comparing again the correlation and relaxation contributions to the EAs shown in Fig. 7. Here one can see that throughout the relaxation contribution strongly dominates over the correlation contribution; see also Sec. IV B. Both the MBPT2 and the RPA and RPAX2 Green's-function methods are able to correct the deficiencies of Koopman's theorem in the description of bound anions as one can see in Fig. 6. Also, it can be seen in the figure that the relative deviations between the MBPT2 values and the RPA or RPAX2 values are less strong than

for the IPs. Significant deviations of 0.4–0.7 eV of the EAs of the Green's-function methods to the CCSD(T) references values are observed for the fluorine molecule (structure 5). Here all propagator methods predict a wrong sign for the EA, i.e., describe an unbound electron in the negatively charged system. Since with Koopman's theorem one obtains a quite strong negative EA for F_2, see Fig. 6, one can conclude that the relaxation contributions obtained by the RPA and RPAX2 propagator methods are too low in magnitude to shift the EA to a positive value and match the CCSD(T) reference result. It was found that similar deviations are also obtained with the second- and third-order OVGF methods; see Supplemental Material [74].

Error statistical values for the different methods considered in this work with respect to the CCSD(T) reference IPs and EAs for the GW27 molecules are shown in Figs. 8 and 9. In the case of the IPs, Fig. 8, one can observe that the RPA and RPAX2 Green's-function approaches yield ionization energies which are closer to the reference results than the corresponding values obtained with the RPA and RPAX2 energy difference methods. The only exception to this is found for the RPA GF method which excludes the static self-energy contributions described in Sec. II B 4. Overall the errors for the IPs yielded by the RPA and also OVGF(3) Green's-function methods are comparable to the MP2 errors while a clear deterioration in the performance is found for the second-order methods MBPT2 and OVGF(2). The analysis above in this section indicates that this behavior mainly stems from an improper description of the correlation part to the self-energy by these methods.

For the EAs almost identical error statistics for the different Green's-function methods are observed, see Table III. This again may be explained by the fact that the corrections to Koopman's theorem mainly originate from the relaxation rather than the correlation contributions; see also Fig. 7. The former appear to be less dependent on the third- and higher-order corrections to the self-energy. A comparison to the different energy difference methods shows that both the MP2 and CCSD methods deliver a higher accuracy for the EAs than the different propagator methods.

V. SUMMARY

A many-body Green's-function method using an infinite-order expansion of ring-type diagram contributions to the self-energy has been presented in this work. The computational approach used herein relates to the density-fitting method for solving the random-phase approximation (RPA) Riccati-type amplitude equation of Ref. [59]. Exchange particle-hole interactions were accounted for by an antisymmetrization of the amplitudes in each iteration of the amplitude update, leading to self-energy contributions that are compatible with the RPAX2 method of Ref. [59].

The methods derived in this work have been used for describing the ionization energies and electron affinities of the molecules from the GW27 database. A comparison to accurate coupled-cluster singles and doubles with perturbative triples [CCSD(T)] reference results has revealed a fairly good performance of the RPA Green's-function (GF) method, comparable to the third-order OVGF method and significantly better than second-order approximations to the many-body GF.

An analysis of the different contributions to the self-energy, namely correlation, relaxation, and static contributions, has shown that a strong cancellation of correlation and relaxation effects occurs for the occupied energy levels, while in the case of the low-lying virtual levels it was found that electron correlation effects to the self-energy are small and that here usually the relaxation energy component dominates. For the molecules considered in this work, in a few cases the relaxation energy contribution to the quasiparticle energies even lead to a sign change of the electron affinity compared to Koopman's theorem, describing a stabilization of the $(N+1)$-electron system relative to the neutral one. This was observed, e.g., for the anthracene molecule and the gold tetramer. The static self-energy contributions were shown to be relatively small in comparison to the correlation and relaxation component.

The comparison between the decompositions of the self-energy into its contributions for the RPA and RPAX2 method has shown that the RPA method overestimates both contributions in magnitude relative to the RPAX2 method. Since the two contributions are opposite in sign, the deviation between the RPA and RPAX2 energy levels is strongly quenched and the total quasiparticle energies are very similar for the two methods.

The vertical coupled-cluster ionization energies and electron affinities derived in this work have been corrected by adding deformation energies of the cations or anions as well as the corresponding energy differences for the zero-point vibrational energies of the neutral and the charged systems. The adiabatic CCSD(T) values obtained in this way were shown to be in a very good agreement with experimental results. They may therefore serve well as a reference to test other electron correlation methods and Green's-function approaches not considered in this work.

The methods derived in this work are based on a diagonal and non-self-consistent approximation to the self-energy matrix. In the future it seems worthwhile to investigate the performance of the approaches without these two constraints. In the case of the former, the diagonal approximation, an inclusion of the occupied-virtual blocks of the self-energy matrix would lead to orbital rotations fulfilling the Brillouin-Brueckner condition and the solutions to the resulting one-particle eigenvalue equations would be Brueckner orbitals compatible with the RPA and RPAX2 wave functions [41,78,79,87,89,146]. A corresponding one-particle Brueckner correlation method has been developed by Beste and Bartlett using a second-order Hamiltonian [39,73]. This method was shown to yield reasonable results for ionization energies, electron affinities, and electric molecular properties [39]. It can therefore be anticipated that the imposition of the Brueckner condition would augment the accuracy also of the RPA methods of this work.

ACKNOWLEDGMENTS

Financial support of this work through the DFG (Deutsche Forschungsgemeinschaft) priority program SPP1807 ("Control of London dispersion interactions in molecular chemistry") is gratefully acknowledged.

[1] N. C. V. Costa, D. R. Lloyd, and P. J. Roberts, J. Chem. Soc. Faraday Trans. **77**, 899 (1981).
[2] B.-M. Cheng, E. P. Chew, C.-P. Liu, J.-S. K. Yu, and C. Yu, J. Chem. Phys. **110**, 4757 (1999).
[3] J. Liu, E. J. Salumbides, U. Hollenstein, J. C. J. Koelemeij, K. S. E. Eikema, and W. Ubachs, J. Chem. Phys. **130**, 174306 (2009).
[4] O. Echt, T. Fiegele, M. Rümmele, M. Probst, S. Matt-leubner, J. Urban, P. Mach, J. Leszcynski, P. Scheier, and T. D. Märk, J. Chem. Phys. **123**, 084313 (2005).
[5] S. Denifl, M. Stano, A. Stamatovic, P. Scheier, and T. D. Märk, J. Chem. Phys. **124**, 054320 (2006).
[6] J. Linderberg and Y. Öhrn, *Propagators in Quantum Chemistry*, 2nd ed. (Wiley-Interscience, Hoboken, NJ, 2004).
[7] L. S. Cederbaum, Theor. Chim. Acta **31**, 239 (1973).
[8] L. S. Cederbaum and W. Domcke, Adv. Chem. Phys. **36**, 205 (1977).
[9] P. Jørgensen and J. Simons, J. Chem. Phys. **63**, 5302 (1975).
[10] J. Linderberg and Y. Öhrn, Int. J. Quantum Chem. **12**, 161 (1977).
[11] Y. Öhrn and J. Linderberg, Int. J. Quantum Chem. **15**, 343 (1979).
[12] Y. Öhrn and G. Born, Adv. Quantum Chem. **13**, 1 (1981).
[13] J. von Niessen, J. Schirmer, and L. S. Cederbaum, Comput. Phys. Rep. **1**, 57 (1984).
[14] J. Oddershede, Adv. Chem. Phys. **69**, 201 (1987).
[15] J. V. Ortiz, J. Chem. Phys. **89**, 6348 (1988).
[16] A. Tarantelli and L. S. Cederbaum, Phys. Rev. A **39**, 1656 (1989).
[17] J. V. Ortiz, Int. J. Quantum Chem., Quant. Chem. Symp. **36**(Suppl. S23), 321 (1989).
[18] V. G. Zakrzewski and J. V. Ortiz, Int. J. Quantum Chem. **53**, 583 (1995).
[19] J. V. Ortiz, J. Chem. Phys. **103**, 5630 (1995).
[20] B. Holm, Phys. Rev. Lett. **83**, 788 (1999).
[21] P. Sanchez-Friera and R. W. Godby, Phys. Rev. Lett. **85**, 5611 (2000).
[22] A. Schleife, F. Fuchs, C. Rödl, J. Furthmüller, and F. Bechstedt, Phys. Status Solidi **246**, 2150 (2009).
[23] G. Onida, L. Reining, R. W. Godby, R. Del Sole, and W. Andreoni, Phys. Rev. Lett. **75**, 818 (1995).
[24] J. Oddershede, Adv. Quantum Chem. **11**, 275 (1978).
[25] S. Baroni, P. Giannozzi, and A. Testa, Phys. Rev. Lett. **58**, 1861 (1987).
[26] K. Sturm and A. Gusarov, Phys. Rev. B **62**, 16474 (2000).
[27] A. Szabo and N. S. Ostlund, *Modern Quantum Chemistry* (Dover, New York, 1996).
[28] R. D. Mattuck, *A Guide to Feynman Diagrams in the Many-body Problem* (Dover, New York, 1992).
[29] J. Simons and P. Jørgensen, J. Chem. Phys. **64**, 1413 (1976).
[30] J. D. Doll and W. P. Reinhardt, J. Chem. Phys. **57**, 1169 (1972).
[31] B. T. Pickup and O. Goscinski, Mol. Phys. **26**, 1013 (1973).
[32] M. E. Casida and D. P. Chong, Chem. Phys. **133**, 47 (1989).
[33] D. Van Neck, K. Peirs, and M. Waroquier, J. Chem. Phys. **115**, 15 (2001).
[34] J. V. Ortiz, J. Chem. Phys. **104**, 7599 (1996).
[35] J. V. Ortiz, Int. J. Quantum Chem. Symp. **22**, 431 (1988).
[36] J. V. Ortiz, Int. J. Quantum Chem. **105**, 803 (2005).
[37] M. Nooijen and J. G. Snijders, Int. J. Quantum Chem. **26**, 55 (1992).
[38] M. Nooijen and J. G. Snijders, Int. J. Quantum Chem. **48**, 15 (1993).
[39] A. Beste and R. J. Bartlett, J. Chem. Phys. **120**, 8395 (2004).
[40] L. Z. Stolarczyk and H. J. Monkhorst, Phys. Rev. A **32**, 725 (1985).
[41] I. Lindgren, in *Fundamental World of Quantum Chemistry*, Vol. 3, edited by E. J. Brändas and E. S. Kryachko (Springer, Berlin, Heidelberg, 2004), pp. 215–245.
[42] J. V. Ortiz, Int. J. Quantum Chem. **100**, 1131 (2004).
[43] L. Hedin, Phys. Rev. **139**, A796 (1965).
[44] F. Aryasetiawan and O. Gunnarsson, Rep. Prog. Phys. **61**, 237 (1998).
[45] H. J. Monkhorst, Adv. Quantum Chem. **48**, 35 (2005).
[46] G. Onida, L. Reining, and A. Rubio, Rev. Mod. Phys. **74**, 601 (2002).
[47] A. Stan, N. E. Dahlen, and R. van Leeuwen, J. Chem. Phys. **130**, 114105 (2009).
[48] D. P. Chong, O. V. Gritsenko, and E. J. Baerends, J. Chem. Phys. **116**, 1760 (2002).
[49] O. Gritsenko and E. J. Baerends, J. Chem. Phys. **121**, 655 (2004).
[50] M. M. Rieger, L. Steinbeck, I. D. White, H. N. Rojas, and R. W. Godby, Comput. Phys. Commun. **117**, 211 (1999).
[51] C. Buth, U. Birkenheuer, M. Albrecht, and P. Fulde, Phys. Rev. B **72**, 195107 (2005).
[52] Y. Shigeta, A. M. Ferreira, V. G. Zakrzewski, and J. V. Ortiz, Int. J. Quantum Chem. **85**, 411 (2001).
[53] M. J. van Setten, F. Weigend, and F. Evers, J. Chem. Theory Comput. **9**, 232 (2013).
[54] M. J. van Setten, F. Caruso, S. Sharifzadeh, X. Ren, M. Scheffler, F. Liu, J. Lischner, L. Lin, J. R. Deslippe, S. G. L. C. Yang, F. Weigend, J. B. Neaton, F. Evers, and P. Rinke, J. Chem. Theory Comput. **11**, 5665 (2015).
[55] F. Caruso, M. Dauth, M. J. van Setten, and P. Rinke, J. Chem. Theory Comput. **12**, 5076 (2016).
[56] E. Maggio, P. Liu, M. J. van Setten, and G. Kresse, J. Chem. Theory Comput. **13**, 635 (2017).
[57] C. Rostgaard, K. W. Jacobsen, and K. S. Thygesen, Phys. Rev. B **81**, 085103 (2010).
[58] P. Koval, D. Foerster, and D. Sanchez-Portal, Phys. Rev. B **89**, 155417 (2014).
[59] A. Heßelmann, Phys. Rev. A **85**, 012517 (2012).
[60] A. Heßelmann, in *Density Functionals: Thermochemistry*, Topics in Current Chemistry Volume 365 (Springer, Heidelberg, 2014), pp. 97–144.
[61] D. J. Tozer and N. C. Handy, J. Chem. Phys. **109**, 10180 (1998).
[62] M. E. Casida, J. Mol. Struct.: THEOCHEM **914**, 3 (2009).
[63] M. Grüning, O. V. Gritsenko, S. J. A. van Gisbergen, and E. J. Baerends, J. Chem. Phys. **114**, 652 (2001).
[64] M. Grüning, O. V. Gritsenko, S. J. A. van Gisbergen, and E. J. Baerends, J. Chem. Phys. **116**, 9591 (2002).
[65] Q. Wu, P. W. Ayers, and W. Yang, J. Chem. Phys. **119**, 2978 (2003).
[66] R. J. Bartlett, I. Grabowski, S. Hirata, and S. Ivanov, J. Chem. Phys. **122**, 034104 (2005).
[67] I. V. Schweigert, V. F. Lotrich, and R. J. Bartlett, J. Chem. Phys. **125**, 104108 (2006).
[68] A. Heßelmann, J. Chem. Phys. **122**, 244108 (2005).
[69] A. Heßelmann, Phys. Chem. Chem. Phys. **8**, 563 (2006).
[70] P. Verma and R. J. Bartlett, J. Chem. Phys. **136**, 044105 (2012).

[71] J. Klimes and G. Kresse, J. Chem. Phys. **140**, 054516 (2014).

[72] F. Kaplan, F. Weigend, F. Evers, and M. J. van Setten, J. Chem. Theory Comput. **11**, 5152 (2015).

[73] A. Beste and R. J. Bartlett, J. Chem. Phys. **123**, 154103 (2005).

[74] See Supplemental Material at http://link.aps.org/supplemental/10.1103/PhysRevA.95.062513 for IPs and EAs for the different methods as well as geometries for the neutral and charged molecules from the GW27 database.

[75] F. Weigend, Phys. Chem. Chem. Phys. **4**, 4285 (2002).

[76] A. Heßelmann, J. Chem. Phys. **146**, 174110 (2017).

[77] F. E. Harris, H. J. Monkhorst, and D. L. Freeman, *Algebraic and Diagrammatic Methods in Many-Fermion Theory* (Oxford University Press, New York,1992).

[78] I. Shavitt and R. J. Bartlett, *Many-Body Methods in Chemistry and Physics: MBPT and Coupled-Cluster Theory* (Cambridge University Press, Cambridge, England, 2009).

[79] I. Lindgren, *Atomic Many-Body Theory* (Springer, Berlin, Heidelberg, 1986).

[80] S. A. Kucharski and R. J. Bartlett, Adv. Quantum Chem. **18**, 281 (1986).

[81] D. L. Freeman, Phys. Rev. B **15**, 5512 (1977).

[82] G. E. Scuseria, T. M. Henderson, and D. C. Sorensen, J. Chem. Phys. **129**, 231101 (2008).

[83] M. Hellgren and U. von Barth, Phys. Rev. B **78**, 115107 (2008).

[84] P. Bleiziffer, A. Heßelmann, and A. Görling, J. Chem. Phys. **139**, 084113 (2013).

[85] A. Grüneis, M. Marsman, J. Harl, L. Schimka, and G. Kresse, J. Chem. Phys. **131**, 154115 (2009).

[86] G. Born, H. A. Kurtz, and Y. Öhrn, J. Chem. Phys. **68**, 74 (1978).

[87] L. Z. Stolarczyk and H. J. Monkhorst, Int. J. Quantum Chem. Symp. **18**, 267 (1984).

[88] S.-S. Liaw, Chin. J. Phys. **32**, 835 (1994).

[89] I. Lindgren, Int. J. Quantum Chem. **90**, 294 (2002).

[90] R. Ahlrichs, M. Bär, M. Häser, H. Horn, and C. Kölmel, Chem. Phys. Lett. **162**, 165 (1989).

[91] A. D. Becke, Phys. Rev. A **38**, 3098 (1988).

[92] J. P. Perdew, Phys. Rev. B **33**, 8822 (1986).

[93] T. H. Dunning, J. Chem. Phys. **90**, 1007 (1989).

[94] R. A. Kendall, T. H. Dunning, Jr., and R. J. Harrison, J. Chem. Phys. **96**, 6796 (1992).

[95] D. Woon and T. H. Dunning, Jr., J. Chem. Phys. **98**, 1358 (1993).

[96] D. Woon and T. H. Dunning, Jr., J. Chem. Phys. **100**, 2975 (1994).

[97] F. Weigend and R. Ahlrichs, Phys. Chem. Chem. Phys. **7**, 3297 (2005).

[98] D. Andrae, U. Haessermann, M. Dolg, H. Stoll, and H. Preuss, Theor. Chim. Acta **77**, 123 (1990).

[99] W. H. E. Schwarz, J. Electron. Spectrosc. Relat. Phenom. **6**, 377 (1975).

[100] A. D. Becke, J. Chem. Phys. **98**, 1372 (1993).

[101] C. Lee, W. Yang, and R. G. Parr, Phys. Rev. B **37**, 785 (1988).

[102] M. J. Frisch, G. W. Trucks, H. B. Schlegel, G. E. Scuseria, M. A. Robb, J. R. Cheeseman, J. A. Montgomery, Jr., T. Vreven, K. N. Kudin, J. C. Burant, J. M. Millam, S. S. Iyengar, J. Tomasi, V. Barone, B. Mennucci, M. Cossi, G. Scalmani, N. Rega, G. A. Petersson, H. Nakatsuji, M. Hada, M. Ehara, K. Toyota, R. Fukuda, J. Hasegawa, M. Ishida, T. Nakajima, Y. Honda, O. Kitao, H. Nakai, M. Klene, X. Li, J. E. Knox, H. P. Hratchian, J. B. Cross, V. Bakken, C. Adamo, J. Jaramillo, R. Gomperts, R. E. Stratmann, O. Yazyev, A. J. Austin, R. Cammi, C. Pomelli, J. W. Ochterski, P. Y. Ayala, K. Morokuma, G. A. Voth, P. Salvador, J. J. Dannenberg, V. G. Zakrzewski, S. Dapprich, A. D. Daniels, M. C. Strain, O. Farkas, D. K. Malick, A. D. Rabuck, K. Raghavachari, J. B. Foresman, J. V. Ortiz, Q. Cui, A. G. Baboul, S. Clifford, J. Cioslowski, B. B. Stefanov, G. Liu, A. Liashenko, P. Piskorz, I. Komaromi, R. L. Martin, D. J. Fox, T. Keith, M. A. Al-Laham, C. Y. Peng, A. Nanayakkara, M. Challacombe, P. M. W. Gill, B. Johnson, W. Chen, M. W. Wong, C. Gonzalez, and J. A. Pople, *Gaussian09 Revision A.02, 2009* (Gaussian Inc., Wallingford, CT, 2016).

[103] H.-J. Werner, P. J. Knowles, G. Knizia, F. R. Manby, M. Schütz, P. Celani, T. Korona, R. Lindh, A. Mitrushenkov, G. Rauhut, K. R. Shamasundar, T. B. Adler, R. D. Amos, A. Bernhardsson, A. Berning, D. L. Cooper, M. J. O. Deegan, A. J. Dobbyn, F. Eckert, E. Goll, C. Hampel, A. Hesselmann, G. Hetzer, T. Hrenar, G. Jansen, C. Köppl, Y. Liu, A. W. Lloyd, R. A. Mata, A. J. May, S. J. McNicholas, W. Meyer, M. E. Mura, A. Nicklass, D. P. O'Neill, P. Palmieri, D. Peng, K. Pflüger, R. Pitzer, M. Reiher, T. Shiozaki, H. Stoll, A. J. Stone, R. Tarroni, T. Thorsteinsson, and M. Wang, Molpro, version 2015.1, a package of ab initio programs, 2012, see http://www.molpro.net.

[104] H.-J. Werner, P. J. Knowles, G. Knizia, F. R. Manby, and M. Schütz, WIREs Comput. Mol. Sci. **2**, 242 (2012).

[105] A. Heßelmann, *Noncovalent Interactions in Quantum Chemistry and Physics: Theory and Applications* (Elsevier, Amsterdam, 2017), Chap. 3.

[106] F. Weigend, F. Furche, and R. Ahlrichs, J. Chem. Phys. **119**, 12753 (2003).

[107] K. L. Bak, P. Jørgensen, J. Olsen, T. Helgaker, and W. Klopper, J. Chem. Phys. **112**, 9229 (2000).

[108] P. Jurecka and P. Hobza, Chem. Phys. Lett. **365**, 89 (2002).

[109] M. S. Marshall, L. A. Burns, and C. D. Sherrill, J. Chem. Phys. **135**, 194102 (2011).

[110] F. Weigend, A. Köhn, and C. Hättig, J. Chem. Phys. **116**, 3175 (2002).

[111] F. Weigend, M. Häser, H. Patzelt, and R. Ahlrichs, Chem. Phys. Lett. **294**, 143 (1998).

[112] D. Shiner, J. M. Gilligan, B. M. Cook, and W. Lichten, Phys. Rev. A **47**, 4042 (1993).

[113] M. W. McGeogh and R. E. Schlier, Chem. Phys. Lett. **99**, 347 (1983).

[114] M. M. Kappes, P. Radi, M. Schar, and E. Schumacher, Chem. Phys. Lett. **113**, 243 (1985).

[115] H. Van Lonkhuyzen and C. A. De Lange, Chem. Phys. **89**, 313 (1984).

[116] T. Trickl, E. F. Cromwell, Y. T. Lee, and A. Kung, J. Chem. Phys. **91**, 6006 (1989).

[117] J. M. Dyke, C. Kirby, and A. Morris, J. Chem. Soc. Faraday Trans. **79**, 483 (1983).

[118] L. Wang, J. E. Reutt, Y. T. Lee, and D. A. Shirley, J. Electron Spectrosc. Relat. Phenom. **47**, 167 (1988).

[119] R. H. Page, R. J. Larkin, Y. R. Yhen, and Y. T. Lee, J. Chem. Phys. **88**, 2249 (1988).

[120] G. Reiser, W. Habenicht, and K. Müller-Dethlefs, J. Chem. Phys. **98**, 8462 (1993).

[121] S. K. Shina, R. R. Corderman, and J. L. Beauchamp, Int. J. Mass Spectrom. Ion Processes **101**, 257 (1990).

[122] D. L. Hildebrand, J. Phys. Chem. **77**, 897 (1973).
[123] C. A. Stearns and F. J. Kohl, J. Phys. Chem. **77**, 136 (1973).
[124] G. Bieri, F. Burger, E. Heilbronner, and J. P. Maier, Helv. Chim. Acta **60**, 2213 (1977).
[125] P. Plessis and P. Marmet, Can. J. Chem. **65**, 1424 (1987).
[126] C. D. Finney and A. G. Harrison, Int. J. Mass Spectrom. Ion Phys. **9**, 221 (1972).
[127] G. D. Flesch and H. J. Svec, J. Chem. Soc. Faraday Trans. **69**, 1187 (1973).
[128] B. A. Williams and T. A. Cool, J. Chem. Phys. **94**, 6358 (1991).
[129] W. M. Trott, N. C. Blais and E. A. Walters, J. Chem. Phys. **69**, 3150 (1978).
[130] H. Van Dam and A. Oskam, J. Electron Spectrosc. Relat. Phenom. **13**, 273 (1978).
[131] G. I. Nemeth, H. L. Selzle, and E. W. Schlag, Chem. Phys. Lett. **215**, 151 (1993).
[132] M. C. R. Cockett, H. Ozeki, K. Okuyama, and K. Kimura, J. Chem. Phys. **98**, 7763 (1993).
[133] J. W. Hager and S. C. Wallace, Anal. Chem. **60**, 5 (1988).
[134] D. Stahl and F. Maquin, Chem. Phys. Lett. **108**, 613 (1984).
[135] K. M. McHugh, J. G. Eaton, G. H. Lee, H. W. Sarkas, L. H. Kidder, J. T. Snodgrass, M. R. Manaa, and K. H. Bowen, J. Chem. Phys. **91**, 3792 (1989).
[136] A. Artau, K. E. Nizzi, B. T. Hill, L. S. Sunderlin, and P. G. Wenthold, J. Am. Chem. Soc. **122**, 10667 (2000).
[137] H. W. Sarkas, J. H. Hendricks, S. T. Arnold, and K. H. Bowen, J. Chem. Phys. **100**, 1884 (1994).
[138] A. A. Viggiano, T. M. Miller, A. E. S. Miller, R. A. Morris, J. M. Van Doren, and J. F. Paulson, Int. J. Mass Spectrom. Ion Processes **109**, 327 (1991).
[139] H.-J. Zhai, B. Kiran, and L.-S. Wang, J. Chem. Phys. **121**, 8231 (2004).
[140] Z. L. Liu, Z. B. Quin, H. Xie, R. Cong, X. Wu, and Z. C. Tang, J. Chem. Phys. **139**, 094306 (2013).
[141] J. Schiedt, W. J. Knott, K. Le Barbu, E. W. Schlag, and R. Weinkauf, J. Chem. Phys. **113**, 9470 (2000).
[142] N. Ando, M. Mitsui, and A. Nakajima, J. Chem. Phys. **127**, 234305 (2007).
[143] K. Krause, M. E. Harding, and W. Klopper, Mol. Phys. **113**, 1952 (2015).
[144] National Institute of Standards and Technology, NIST chemistry WebBook, 2016, http://webbook.nist.gov/.
[145] R. N. Compton, P. W. Reinhardt, and C. D. Cooper, J. Chem. Phys. **63**, 3821 (1975).
[146] R. J. Bartlett, Chem. Phys. Lett. **484**, 1 (2009).